ACS Biomaterials SCIENCE & ENGINEERING

Article

pubs.acs.org/journal/abseba

Critical Length of PEG Grafts on lPEI/DNA Nanoparticles for Efficient in Vivo Delivery

John-Michael Williford,[†,‡,§] Maani M. Archang,[†,§,⊥] Il Minn,[∥] Yong Ren,[§,⊥] Mark Wo,[§,⊥] John Vandermark,[§,⊥] Paul B. Fisher,[△,○,□] Martin G. Pomper,[§,⊥,∥] and Hai-Quan Mao*[,§,⊥,#]

[‡]Department of Biomedical Engineering, Johns Hopkins University School of Medicine, 720 Rutland Avenue, Baltimore, Maryland 21205, United States

[§]Institute for NanoBioTechnology and [⊥]Department of Materials Science and Engineering, Johns Hopkins University, 3400 N. Charles Street, Baltimore, Maryland 21218, United States

[∥]Russell H. Morgan Department of Radiology and Radiological Sciences, Johns Hopkins Medical Institutions, 601 N. Caroline Street, Baltimore, Maryland 21287, United States

[#]Translational Tissue Engineering Center and Whitaker Biomedical Engineering Institute, Johns Hopkins University School of Medicine, 400 N. Broadway, Baltimore, Maryland 21287, United States

[△]Department of Human and Molecular Genetics, Virginia Commonwealth University, 1101 East Marshall Street, Richmond, Virginia 23298, United States

[○]VCU Institute of Molecular Medicine, Virginia Commonwealth University, 1220 East Broad Street, Richmond, Virginia 23298, United States

[□]VCU Massey Cancer Center, Virginia Commonwealth University, 401 College Street, Richmond, Virginia 23298, United States

S *Supporting Information*

ABSTRACT: Nanoparticle-mediated gene delivery is a promising alternative to viral methods; however, its use in vivo, particularly following systemic injection, has suffered from poor delivery efficiency. Although PEGylation of nanoparticles has been successfully demonstrated as a strategy to enhance colloidal stability, its success in improving delivery efficiency has been limited, largely due to reduced cell binding and uptake, leading to poor transfection efficiency. Here we identified an optimized PEGylation scheme for DNA micellar nanoparticles that delivers balanced colloidal stability and transfection activity. Using linear polyethylenimine (lPEI)-*g*-PEG as a carrier, we characterized the effect of graft length and density of polyethylene glycol (PEG) on nanoparticle assembly, micelle stability, and gene delivery efficiency. Through variation of PEG grafting degree, lPEI with short PEG grafts (molecular weight, MW 500−700 Da) generated micellar nanoparticles with various shapes including spherical, rodlike, and wormlike nanoparticles. DNA micellar nanoparticles prepared with short PEG grafts showed comparable colloidal stability in salt and serum-containing media to those prepared with longer PEG grafts (MW 2 kDa). Corresponding to this trend, nanoparticles prepared with short PEG grafts displayed significantly higher in vitro transfection efficiency compared to those with longer PEG grafts. More importantly, short PEG grafts permitted marked increase in transfection efficiency following ligand conjugation to the PEG terminal in metastatic prostate cancer-bearing mice. This study identifies that lPEI-*g*-PEG with short PEG grafts (MW 500−700 Da) is the most effective to ensure shape control and deliver high colloidal stability, transfection activity, and ligand effect for DNA nanoparticles in vitro and in vivo following intravenous administration.

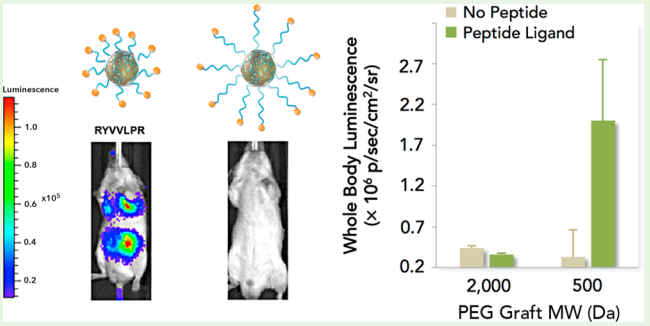

KEYWORDS: *nonviral, tumor-specific promoter, DNA, nanomedicine, shape*

INTRODUCTION

Gene therapy remains exciting as a therapeutic strategy for a number human diseases, including cancer, metabolic disorders, and immune deficiencies.[1−4] Although virus-based methods have largely been employed for these applications, evident by their use in approximately 70% of gene therapy clinical trials to date,[1] safety concerns motivate the need to engineer alternative gene delivery systems.[5] Nonviral gene delivery strategies have been developed to overcome these significant limitations posed by viral vectors, namely the potential for immune responses,

Received: December 22, 2015
Accepted: March 2, 2016
Published: March 3, 2016

DOI: 10.1021/acsbiomaterials.5b00551
ACS Biomater. Sci. Eng. 2016, 2, 567−578

carcinogenesis based on site-specific integration, limited DNA payload size, and difficulty of large-scale vector production.[5−9] Nanoparticles comprise the main class of nonviral carriers, because of their ability to protect the DNA from degradation, target specific cells and tissues, and improve intracellular delivery of the payload.[3,10−14]

Cationic polymers are commonly used to condense plasmid DNA into nanoparticles through electrostatic interactions.[3,15−17] Polymeric nanoparticles effectively deliver genetic material in vitro, although their performance in vivo has demonstrated varying degrees of efficacy following intravenous administration, often showing transgene expression primarily in the lung.[18,19] These mixed results are likely due to the interaction between cationic nanoparticles and serum components, leading to rapid aggregation, entrapment in capillary beds, and/or capture and clearance by the mononuclear phagocytic system (MPS).[20−23] Of the numerous polymers developed for gene therapy applications, linear polyethylenimine (lPEI) remains one of the most popular because of its demonstrated efficiency in both cell culture and various animal models,[24,25] particularly following local administration,[26−28] although it still suffers from aggregation issues in physiological media.[29,30]

Surface coating of polymer/DNA nanoparticles has been widely used to improve their stability in biological environments, such as those encountered following systemic administration. One popular surface coating strategy has been PEGylation, typically through the use of block or graft copolymers comprised of a polycation chain and a polyethylene glycol (PEG) chain to form a core−shell, polyelectrolyte complex micelle assembly.[15,31] PEGylated nanoparticles demonstrate enhanced stability in serum, reducing aggregation, increasing circulation time, and decreasing MPS clearance after intravenous injection.[32−34]

In addition to the stability improvements conferred by PEGylation, recent work has highlighted the importance of PEG in the ability to control the shape of polymer/DNA nanoparticles for gene therapy applications. For example, using a PEG-polyphosphoramidate (PPA) block copolymer, DNA nanoparticle shape can be controlled through variation of solvent polarity during nanoparticle formation, ranging from spherical to rodlike and wormlike shapes.[35] Experimental studies and molecular dynamics simulations highlighted the important role of PEG in shape formation, as particles prepared without the PEG block did not demonstrate an ability to tune the shape of polymer/DNA micelles. We have recently observed similar results for PEG-polycation graft copolymers, including PPA and lPEI, where increasing the PEG grafting degree led to shape variation from more condensed spherical and short rod shapes to longer rod- and wormlike shapes.[36,37]

Although PEGylation provides significant benefits during circulation and transport of nanoparticle delivery systems, several drawbacks exist for successful gene delivery both in vitro and in vivo. The dense PEG layer and accompanying near-neutral surface charge significantly decreases interaction with the target cells of interest.[38−40] Because of the lowered cell uptake, transgene expression mediated by PEGylated nanoparticles has been observed to drop by several orders of magnitude.[39]

In order to minimize the drop in transfection efficiency associated with PEG-polycation/DNA nanoparticles, we hypothesized that small molecular weight PEG chains could be utilized to maintain nanoparticle colloidal stability in physiological media without significantly reducing its effectiveness as a gene delivery vehicle. In addition, previous results suggest that with sufficient PEG grafting degree, shorter PEG chains may still be used to control the shape of polymer/DNA nanoparticles,[37] a potential important parameter for in vivo application given the demonstrated importance of nanoparticle shape on cellular uptake, tissue diffusion, and transport properties in several recent studies.[41−44]

Here, we specifically compared the physicochemical properties and transfection ability of nanoparticles prepared with lPEI grafted with PEG with molecular weight of 700 Da (PEG7H) to those of 2000 Da (PEG2K), the minimum PEG length typically recommended to afford the major benefits associated with PEGylation in the literature.[45,46] Many studies use PEG chain lengths much longer than this, ranging from 3400 Da to 20 000 Da for various DNA delivery applications.[32,47−52] Here we report an lPEI-*g*-PEG/DNA nanoparticle system for effective in vivo delivery applications, particularly for the detection of metastatic prostate cancer. A series of lPEI-*g*-PEG carriers with different PEG grafting densities and PEG length (PEG7H and PEG2K) were used to assemble with plasmid DNA, forming various shaped micellar nanoparticles. Their shapes, surface characteristics, and colloidal stability in salt and serum-containing media were correlated with their transfection efficiency in several cell lines, both in the absence and presence of cell adhesion peptides. Optimized carriers were tested following systemic injection in vivo using both Balb/c mice and metastatic prostate cancer-bearing mice. Using these nanoparticles, we demonstrated the ability of short PEG grafts for successful nanoparticle stabilization and efficient in vivo delivery. This work highlights a key design parameter for the development of effective nonviral gene carriers with significant potential for cancer detection and therapy.

MATERIALS AND METHODS

Synthesis and Characterization of lPEI-*g*-PEG Copolymers. Linear polyethylenimine (lPEI, molecular weight 22 kDa, 2.15 mg), *N*-hydroxysulfosuccinimide (sulfo-NHS, 1.09 mg) and functionalized polyethylene glycol acetic acid (X-PEG-COOH, average molecular weight 500, 700, or 2000 Da, X- represents methoxy or SPDP terminal group) with different amounts according to the designed grafting density were dissolved in 1 mL of 0.05 mol/L pH 4.75 phosphate buffer. The pH of solution was monitored and kept in the range of 4.5−5.0 by adding either 1 M HCl or 1 M NaOH solution. 1-Ethyl-3-[3-(dimethylamino)propyl] carbodiimide (EDC) hydrochloride (2.88 mg) was dissolved in 100 μL of ultrapure water and immediately added to the reaction mixture. Another 4 batches of EDC (same quantity) were added every other hour. The final product was purified by ultracentrifugation using a membrane with a molecular weight cutoff (MWCO) of 3500 Da. The ^{1}H NMR spectrum of lPEI-*g*-PEG (2.3%) is shown in Figure S1. PEG grafting degree was characterized by measuring the SPDP content of the polymer. Polymers were treated with 50 mM dithiothreitol solution for 1 h to reduce SPDP, after which the concentration of pyridine 2-thione was measured by UV spectrophotometry at 343 nm according to the manufacturer's protocol (Pierce, Rockford, IL). Grafting density is denoted as a molar percentage of amines in lPEI backbone modified by PEG.

Formation of lPEI-*g*-PEG/DNA Nanoparticles. VR1255C plasmid DNA (6.4 kb) encoding the gene for firefly luciferase driven by the cytomegalovirus promoter was kindly provided by Vical (San Diego, CA). Plasmid DNA was amplified in DH5α *E. coli* and was purified using an EndoFree Giga Kit (Qiagen, Valencia, CA) and dissolved at 1 mg/mL in endotoxin-free TE buffer. For a typical nanoparticle preparation, 10 μg of DNA was diluted in 100 μL of DI water to give a final concentration of 100 μg/mL DNA. A solution of lPEI-*g*-PEG was diluted to 100 μL in DI water to give a final N/P ratio

DOI: 10.1021/acsbiomaterials.5b00551
ACS Biomater. Sci. Eng. 2016, 2, 567−578

(ratio of amine in lPEI to phosphate in DNA) of 8 as used in our previous studies with PEG-polycation/DNA nanoparticles.[35−37] The polymer solution was added to the DNA solution and mixed by rapid pipetting, after which the polymer/DNA mixture was incubated for 10 min prior to further use.

Transmission Electron Microscopy of lPEI-*g*-PEG/DNA Nanoparticles. TEM imaging of nanoparticles was done by incubating 10 μL of lPEI-*g*-PEG/DNA nanoparticle solution onto an ionized nickel grid covered with a carbon film. After 10 min, the solution was removed, and a 6 μL drop of 2% uranyl acetate was added to the grid. After 20 s, the staining solution was removed, and the grid was dried at room temperature. The samples were imaged with a Technai FEI-12 electron microscope. Nanoparticle sizes were characterized from TEM images using ImageJ 1.44. Aspect ratios were determined by dividing the length of the nanoparticle by the diameter. At least 100 nanoparticles were measured from TEM images for each preparation.

lPEI-*g*-PEG/DNA Nanoparticle Zeta Potential Measurement. Nanoparticle zeta potential was measured using a Zetasizer Nano ZS90 (Malvern Instruments, Southborough, MA). An aliquot of 5 μg of DNA nanoparticle solution was diluted to 800 μL with DI water or 150 mM sodium chloride, added to a DTS1070-folded capillary cell, and measured in the automatic mode.

lPEI-*g*-PEG/DNA Nanoparticle Stability Characterization. To test the stability in physiological ionic strength solution, a predetermined volume of 5 M NaCl solution was added to a 5 μg DNA dose nanoparticle solution to give a final NaCl concentration of 150 mM. The mixture solution was incubated for 15 min, and then particle size was measured using dynamic light scattering method with a Zetasizer Nano ZS90. To test the stability in serum, we incubated an aliquot of nanoparticle solution containing 5 μg of DNA with fetal bovine serum (FBS) at a final serum concentration of 5% (v/v) for 15 min before measuring the particle size.

DNA Release from lPEI-*g*-PEG/DNA Nanoparticles. The release of DNA from lPEI-*g*-PEG/DNA nanoparticles was assessed in the presence of heparin sulfate as modified from our previously reported protocol.[53] An aliquot of 20 μL of nanoparticles solution containing 1 μg of DNA was added to each well of a 96-well plate followed by the addition of 80 μL of 1 mg/mL ethidium bromide solution. To this solution, 100 μL of heparin sulfate solution with increasing concentrations in 300 mM NaCl solution was added to each well and mixed thoroughly, giving final heparin sulfate concentrations ranging from 1 μg/mL to 500 μg/mL in 150 mM NaCl. The solutions were incubated at room temperature for 15 min, and the fluorescence intensity (λ_{ex} = 510 nm, λ_{em} = 595 nm) was measured using a fluorescence plate reader (SpectraMax Gemini XPS, Molecular Devices, Sunnyvale, CA). The percentage of DNA released was calculated according to a calibration curve of plasmid DNA subjected to the same conditions.

Ligand Conjugation to lPEI-*g*-PEG/DNA Nanoparticles. Ligands were conjugated to polymer/DNA nanoparticles prepared with SPDP-PEG grafts through SPDP-thiol coupling chemistry. Cyclic RGD-thiol ligand (PCI-3686-PI, Peptides International, Louisville, KY) was dissolved in phosphate buffered saline (PBS) at 1 mg/mL according to the manufacturer's protocol. Peptide 947W (Ac-CCR**RYVVLPR**WLC, ChinaPeptides Co., Ltd., Shanghai, China) was dissolved in PBS at 1 mg/mL. Briefly, lPEI-*g*-PEG(SPDP)/DNA nanoparticles were prepared as described above. Following particle incubation for 10 min, a solution containing the thiolated peptide at a 1:1 thiol:SPDP equivalent molar ratio was added to the nanoparticle solution. The nanoparticles were further incubated for 4 h to allow for peptide conjugation, after which they were used for characterization and testing.

In Vitro Transfection of lPEI-*g*-PEG/DNA Nanoparticles. The base media for maintaining PC3-ML cells,[54] MDA-MB-231 cells, and HeLa cells were F-12K Nutrient Mixture (Kaighn's Modification, Life Technologies, Carlsbad, CA), RPMI-1640 media, and Dulbecco's Modified Eagle's Medium (DMEM), respectively. All media were supplemented with 10% FBS and 100 U/mL Penicillin/100 μg/mL Streptomycin, and cells were cultured at 37 °C and 5% CO_2 in a humidified incubator. At 24 h prior to the transfection experiments, cells were seeded in 48-well plates at a density of 2 × 10^4 cells/well. Various nanoparticle solutions equivalent to 0.5 μg of DNA dose were added to the cells and incubated for 4 h, followed which the media were refreshed. After 48 h, media were removed, and cells were washed with 1 × PBS (pH 7.4). One hundred microliters of reporter lysis buffer (Promega, Madison, WI) was added to each well. Cells were then subjected to two freeze−thaw cycles. Twenty microliters of cell lysate from each well was assayed using a luciferase assay kit (Promega, Madison, WI) on a luminometer (20/20n, Turner BioSystems, Sunnyvale, CA). The luciferase activity was converted to the amount of luciferase expressed using a recombinant luciferase protein (Promega) as the standard and normalized against the total protein content in the lysate using a BCA assay (Pierce, Rockford, IL).

In Vitro Cellular Uptake of lPEI-*g*-PEG/DNA Nanoparticles. Cellular uptake efficiencies were measured in PC3-ML cells using tritium-labeled plasmid DNA. To prepare the radiolabeled DNA, plasmid DNA was methylated with CpG methyl transferase (M.SssL) (New England Biolabs, Ipswich, MA) and S-adenosyl-L-(methyl-3H) methionine (PerkinElmer, Waltham, MA) according to the manufacturer's protocol. Briefly, nuclease-free water, 10× NEB buffer, S-adenosyl-L-(methyl-3H) methionine, plasmid DNA, and M.SssL were mixed in order. The solution was then incubated at 37 °C for 1 h, and the reaction was quenched by heating to 65 °C for 20 min. The radiolabeled DNA was purified using Miniprep Kit (Qiagen, Valencia, CA). Radiolabeled lPEI-*g*-PEG/DNA nanoparticles were prepared as above by mixing radiolabeled DNA with nonradiolabeled DNA at 1/10 DNA weight ratio. At 24 h prior to the transfection experiment, PC3 cells were seeded in 48-well plates at a density of 2 × 10^4 cells/well. Nanoparticles containing 0.5 μg of labeled DNA were added to the cells according to the same protocol as described above in the transfection experiments. After 4 h of incubation, the media in each well was carefully removed, and the cells were washed with 200 μL of PBS. One hundred microliters of reporter lysis buffer was added to each well, and cells were subjected to two freeze−thaw cycles. Cell lysate from each well (50 μL) was added to a scintillation vial and mixed with 4 mL of scintillation fluid. The radioactivity of each sample solution was measured on a liquid scintillation counter (TRI-CARB 1900 TR, Packard, Downers Grove, IL). Cell uptake percentage was calculated by dividing the radioactivity (in DPM) of each sample with the radioactivity of the total dose of nanoparticles added to each well.

In Vivo Transfection of lPEI-*g*-PEG/DNA Nanoparticles. All protocols for the use of animals were approved by the Johns Hopkins Institutional Animal Care and Use Committee. Nanoparticle formulations consisting of 40 μg of a DNA dose in 250 μL of 5% (v/v) glucose were administered via tail vein injection into mice. In vivo jetPEI nanoparticle formulations were prepared at N/P 6 according to the manufacturer's protocol (Polyplus Transfection, France) and used as a positive control for all in vivo experiments. Bioluminescence imaging was performed at predetermined time points. Mice were anesthetized with 2% isoflurane and injected *i.p.* with 100 μL 30 mg/mL D-luciferin solution. Mice were then transferred to an IVIS Spectrum Imaging System (Caliper Life Sciences, Hopkinton, MA) and placed ventral side up. On 3 min intervals after D-luciferin injection, bioluminescence signal was measured for 1 min, until reaching the maximum signal strength. The whole body luciferase expression was calculated using the maximum signal and expressed as radiance (photons/s/cm^2/sr). Gene expression levels were also measured from the major organs following homogenization using a luciferase assay kit. Briefly, mice were anesthetized and sacrificed, and major organs were collected and weighed. Organs were homogenized in 5 mL of PBS each using a tissue homogenizer (Heidolph, Oak Grove, IL) at 15 000 rpm for 15 s intervals. Twenty microliter of tissue lysate from each organ was assayed for gene expression using a luciferase assay kit (Promega, Madison, WI) on a luminometer (20/20n, Turner BioSystems, Sunnyvale, CA) and was normalized to the weight of the tissue sample.

Establishment of Metastatic Prostate Cancer Model. Metastatic prostate cancer model was generated according to our previously established protocol.[54] Briefly, 4 to 6-week old male NOG (NOD/Shi-*scid*/IL-2Rγ^{null}) mice were obtained from the Sidney

DOI: 10.1021/acsbiomaterials.5b00551
ACS Biomater. Sci. Eng. 2016, 2, 567−578

Kimmel Comprehensive Cancer Center Animal Core Facility (Johns Hopkins School of Medicine). PC3-ML cells were expanded over 3 to 5 passages, harvested, and diluted to a concentration of 2×10^7 cells/mL in sterile RPMI-1640 media supplemented with 1% FBS (Life Technologies, Carlsbad, CA). Two hundred μL cell suspension (1×10^6 cells) were administered via the tail vein to establish the metastatic tumor model.

Biodistribution of lPEI-*g*-PEG/DNA Nanoparticles. Nanoparticle biodistribution studies were done in PC3-ML-bearing NOG mice. Tumors were established as described above. Tritium-labeling of DNA was carried out using the previously described protocol. Nanoparticle formulations consisting of 40 μg DNA dose in 250 μL final volume, 5% (v/v) glucose, were administered via tail vein injection into mice. Nanoparticles were formulated at a 1:4 ratio of tritium-labeled DNA to unlabeled DNA. At 2 h after nanoparticle injection, mice were anesthetized and sacrificed, and major organs were harvested, weighed, and solubilized in solvable tissue solubilizing solution (PerkinElmer, Waltham, MA). An aliquot of 200 μL mixture from each organ was added was added to a scintillation vial and mixed with 4 mL of scintillation fluid. The radioactivity of each sample solution was measured on a liquid scintillation counter (TRI-CARB 1900 TR, Packard, Downers Grove, IL). Biodistribution was reported as a percentage of the total injected dose by dividing the calculated radioactivity (in DPM) of each organ with the total radioactivity of the injected nanoparticle formulation.

Toxicity of lPEI-*g*-PEG/DNA Nanoparticles. Liver toxicity was analyzed by measuring serum levels of aspartate aminotransferase (AST) and alanine aminotransferase (ALT). Blood samples were collected from mouse facial vein into serum separator tubes (BD Biosciences, San Jose, CA). Samples were centrifuged at 5000 rpm for 10 min to separate serum. ALT and AST levels were analyzed at the Department of Molecular and Comparative Pathology at Johns Hopkins University. For histopathological evaluation, mice were anesthetized and sacrificed, and major organs (heart, lung, liver, kidney, and spleen) were harvested, fixed in 10% formalin, and tissues were embedded in paraffin blocks. Tissue sections were prepared and stained with hematoxylin and eosin.

Statistical Analysis. All bar graphs represent mean ± standard deviation (SD). Comparison of nanoparticles with PEG graft lengths and comparison of nanoparticles with and without peptide conjugation was conducted using a Student's *t*-test. Differences were considered statistically significant for $p < 0.05$.

RESULTS AND DISCUSSION

Short PEG Grafts Were Sufficient to Confer Shape Control and Maintain Stability. We closely examined linear PEI (lPEI)-*g*-PEG copolymers with different PEG grafts, particularly short grafts with MW < 1 kDa, on their abilities to confer assembly, shape control, colloidal stability, and transfection activity of nanoparticles. Previously, few studies have used PEG chains with MW less than 2 kDa for nanoparticle surface stabilization; PEG 2 kDa has been regarded as the minimum length for nanoparticle stabilization.[46] In a rare report by Petersen et al. on plasmid DNA delivery, a branched polyethylenimine (bPEI)-*g*-PEG copolymer with 35 PEG (550 Da) grafts per PEI chain was used to prepare DNA micellar nanoparticles.[34] Compared to higher molecular weight PEG grafts, 550 Da PEG-grafted bPEI showed the best transfection properties in vitro, albeit lower colloidal stability in serum-containing medium. However, there was no further optimization of the nanoparticles prepared with these short PEG grafts. Because lPEI with an average molecular weight of 22 000 has been widely used for both in vivo and in vitro transfection,[30,46,48,54,55] we prepared a series of $lPEI_{22K}$-*g*-PEG/DNA nanoparticles with two different PEG graft lengths—PEG7H (700 Da) and PEG2K (2000 Da) and various PEG grafting degrees ranging from 0.2 to 2.3% (molar percentage of PEG chains compared to total amount of amines on lPEI). PEGylated nanoparticle formulations were prepared at an N/P ratio of 8, whereas lPEI control nanoparticle formulations were prepared at an N/P ratio of 5. These values were optimized to maximize transfection efficiency while minimizing cytotoxicity (Figure S2). In this study, we kept the grafting density to be relatively low (<3%) based on two considerations. First, we observed that the shape variation of the polymer-DNA micelles occurred in a very narrow range of grafting degrees, 0.2−3%, which is equivalent to about 1−10 PEG grafts per linear PEI chain (22 kDa). Second, when assembled using copolymers with higher grafting degrees (>3%), all nanoparticles assumed warm-like morphology and exhibited background level of transfection efficiency (data not shown). This observation was similar to our previous study with PPA-*g*-PEG/DNA nanoparticles.[37] As the PEG grafting degree increases for both PEG7H and PEG2K grafts, $lPEI_{22K}$-*g*-PEG/DNA nanoparticles underwent a significant shape change (Figure 1) with particles adopting a more condensed spherical and short rod shapes at 0.2% grafting degree, and extending to longer wormlike shape at higher grafting degrees of 1 and 2.3%. Nanoparticle shape transition from spherical to rodlike morphology occurred at slightly lower grafting degree (0.5%) for PEG2K grafts and also led to longer wormlike shapes with higher aspect ratios compared to nanoparticles prepared with

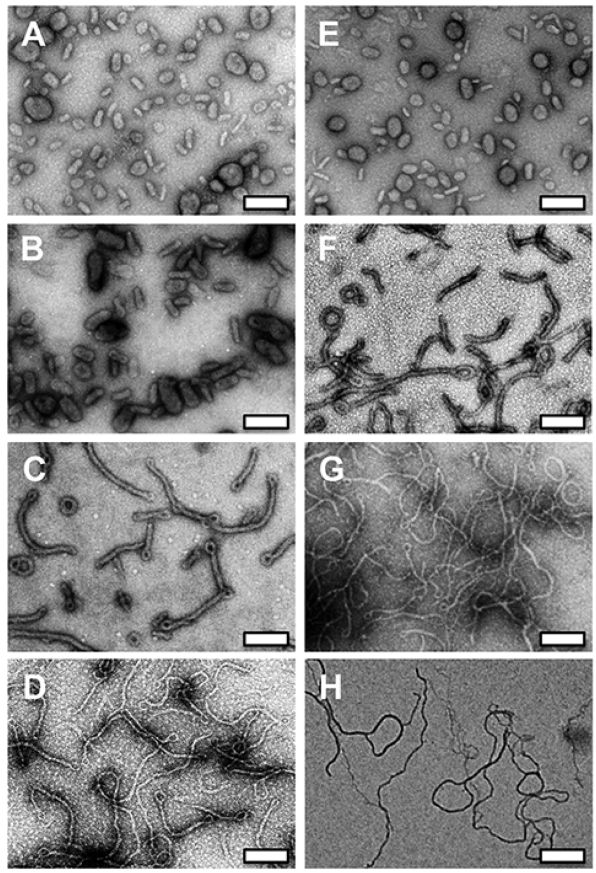

Figure 1. Short PEG grafts allow for $lPEI_{22K}$-*g*-PEG/DNA nanoparticle shape control. TEM images of (A−D) lPEI-*g*-PEG7H/DNA nanoparticles and (E−H) lPEI-*g*-PEG2K/DNA nanoparticles prepared with (A, E) 0.2% PEG grafting degree, (B, F) 0.5% PEG grafting degree, (C, G) 1% PEG grafting degree, and (D, H) 2.3% PEG grafting degree. All scale bars = 200 nm.

DOI: 10.1021/acsbiomaterials.5b00551
ACS Biomater. Sci. Eng. 2016, 2, 567−578

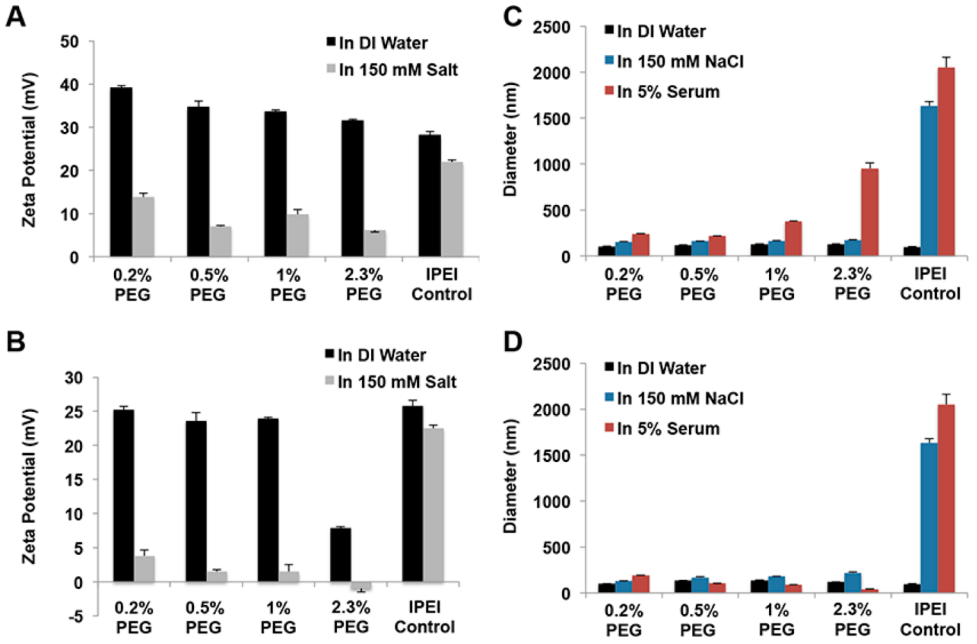

Figure 2. Short PEG grafts maintain stability of polymer/DNA nanoparticles in physiological media. Zeta potential of (A) lPEI-*g*-PEG7H/DNA and (B) lPEI-*g*-PEG2K/DNA nanoparticles at N/P ratio of 8 in DI water and 150 mM NaCl solution in comparison with lPEI/DNA nanoparticles prepared at N/P ratio of 5. Each bar represents mean ± standard deviation (n = 3). Size of (C) lPEI-*g*-PEG7H/DNAand (D) lPEI-*g*-PEG2K/DNA nanoparticles after 15 min incubation in DI water, 150 mM NaCl, and 5% serum, respectively. Each bar represents mean ± standard deviation (n = 3).

PEG7H grafts (Figure 1E−H and Figure S3). These results are consistent with previous results observed for PPA-*g*-PEG/DNA nanoparticles with varying PEG chain lengths, where longer PEG chains led to more elongated nanoparticle shapes at increasing PEG grafting degrees of 2 and 4%.[37] Aspect ratio quantification from the transmission electron microscopy (TEM) images confirmed these trends with nanoparticles prepared with both PEG grafts displayed average aspect ratios of ∼1.5 at 0.2% grafting degree, transitioning to aspect ratios of 20 and 36 at 2.3% grafting degree for PEG7H and PEG2K, respectively (Figure S3).

Next, we measured the surface charge of lPEI-*g*-PEG/DNA nanoparticles in both water and 150 mM salt. Nanoparticles prepared with PEG7H grafts maintained a positive surface charge greater than +30 mV in water; after incubation in salt, however, surface charges dropped significantly to +13 mV for 0.2% grafting degree. We observed similar drops for all PEG7H-grafted polymers, whereas lPEI control particles maintained a positive charge of +22 mV in salt (Figure 2A). These results indicate that short PEG grafts can still significantly mask the positive surface charges in media at physiological ionic strength, even at low grafting degrees. It is important to note that the surface charge of lPEI control particles is lower in water compared to PEG7H-grafted nanoparticles, likely due to the fact that N/P 5 was used for lPEI control particles, whereas N/P 8 was used for PEG-grafted nanoparticles. We observed similar results for DNA nanoparticles complexed by lPEI with PEG2K grafts, albeit the drops in surface charge for these particles were greater after incubation in salt (Figure 2B). This observation can be attributed to stronger charge screening effect from the "thicker" electrostatically neutral corona generated by the longer PEG grafts.

To confirm that the short, PEG7H grafts could improve DNA nanoparticle stability over those prepared with lPEI, we incubated each series of DNA nanoparticles in 5% serum and 150 mM NaCl solution for 15 min. Nanoparticles prepared with both PEG lengths showed significant improvements in the colloidal stability compared to lPEI control particles, which rapidly aggregated from 100 nm in water to 1.6 μm in 0.15 M NaCl solution and 2 μm in 5% serum within the 15 min incubation period (Figure 2C, D). PEG7H-grafted particles showed some size increase in 5% serum, although nanoparticle diameter generally remained below 400 nm, much lower than non-PEGylated lPEI controls. Only 2.3% PEG7H grafts showed significant size increase in serum, although it is possible that this is due to limitations with dynamic light scattering for characterizing nonspherical particles since particles with lower PEG density showed no aggregation. All particles prepared with PEG2K grafts showed no detectable aggregation in salt or serum-containing media.

PEG Graft Length Significantly Influences in Vitro Transfection Efficiency. We evaluated the series of nanoparticles prepared with either PEG7H or PEG2K grafts for their transfection efficiency in vitro using a luciferase-expressing reporter plasmid DNA in three separate cell lines: PC3 prostate cancer cells, MDA-MB-231 breast cancer cells, and HeLa cells. In all cell lines, PEG7H-grafted nanoparticles displayed higher transfection efficiency compared to PEG2K-grafted particles at similar grafting degrees (Figure 3A and Figure S4). For example, in PC3 cells, nanoparticles prepared with 0.2% PEG7H grafts showed nearly 100-fold higher transfection efficiency compared to PEG2K-grafted particles. As the shapes of these two particles are the same, it is likely that PEG chain length is a major determining factor for the difference in gene expression. At grafting degrees of 0.5% or higher, PEG2K-grafted particles mediated near-background levels of gene expression, whereas efficiency of PEG7H-grafted particles was significantly higher. Although PEG2K-grafted nanoparticles had higher aspect ratios, the overall shape of micelles prepared with

DOI: 10.1021/acsbiomaterials.5b00551
ACS Biomater. Sci. Eng. 2016, 2, 567−578

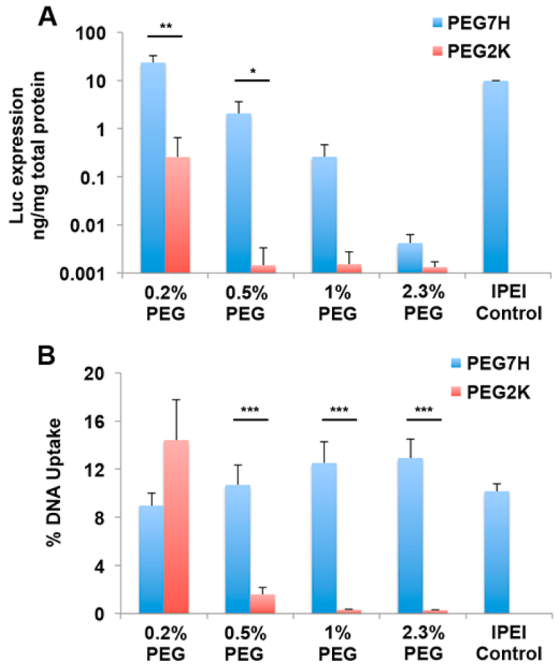

Figure 3. PEG graft length significantly impacts in vitro transfection efficiency. Transfection efficiency (A) and cellular uptake efficiency (B) of lPEI-*g*-PEG7H/DNA and lPEI-*g*-PEG2K/DNA nanoparticles in PC3 cells. Each bar represents mean ± standard deviation ($n = 3$). * $p < 0.05$, ** $p < 0.01$, *** $p < 0.001$.

both PEG grafts was similar, highlighting the contribution of PEG graft length in maintaining high transfection efficiency, besides the grafting density of PEG in copolymer and the aspect ratio of the micelles. Similar trends were observed in both MDA-MB-231 cells and HeLa cells (Figure S4), although the absolute level of gene expression varied between cell lines. Importantly, even the worm-shaped nanoparticles prepared with 2.3% PEG7H grafts exhibited reasonably high level of transfection efficiency in HeLa cells.

To understand the differences in transfection observed with nanoparticles prepared from copolymers with various PEG graft lengths, we evaluated the cellular uptake efficiency of each series of nanoparticles in PC3-ML cells using tritium-labeled DNA (Figure 3B). At 0.2% grafting degree, both PEG7H and PEG2K-grafted nanoparticles exhibited high cellular uptake efficiency. At all other grafting degrees, PEG7H maintained high cellular uptake efficiency, whereas PEG2K decreased cellular uptake to near-background levels. Uptake levels do not always directly correlate with the observed PC3 transfection results, suggesting that other barriers in the delivery process such as endosomal escape, nuclear translocation, and intracellular release of plasmid DNA may play important roles as well. For example, 0.2% PEG2K-grafted nanoparticles showed higher cell uptake but lower gene expression compared to PEG7H-grafted nanoparticles, possibly due to incomplete cellular internalization or poor endosomal escape, two limitations previously associated with longer PEG grafts.[56,57] On the other hand, nanoparticles with PEG7H grafts exhibited similarly high cellular uptake but reduced transfection efficiency at grafting degrees higher than 0.5%. In these cases, the worm-shaped nanoparticles may also suffer from incomplete cellular internalization or less efficienct intracellular trafficking due to their high aspect ratio. An additional contributing factor may be related to the intracellular DNA release. However, as shown in Figure S5, following challenge from varying concentrations of heparin sulfate, nanoparticles at each tested PEG grafting density showed similar DNA release characteristics, regardless of PEG chain length. At higher PEG grafting densities, PEG2K-grafted particles released DNA at slightly lower concentrations of heparin sulfate, indicating higher propensity to release the condensed DNA. As all densities of PEG2K-grafted particles demonstrated lower transfection efficiency compared to PEG7H, it is not likely that DNA release rate represents a major factor affecting transfection ability for these nanoparticles.

PEG Graft Length Significantly Influences Transfection Efficiency of Ligand-Conjugated Nanoparticles. Ligand conjugation to the terminal end of PEG chains is a popular strategy to overcome the reduction in nanoparticle delivery efficiency following PEGylation designed to improve nanoparticle stability, although its effect vary greatly.[58] Here we evaluated the effect of PEG graft length on transfection improvement following ligand conjugation. We prepared a series of lPEI-*g*-PEG/DNA nanoparticles comprised of PEG5H or PEG2K grafts, both containing a terminal 2-pyridyldithio (SPDP) group. PEG5H grafted nanoparticles displayed similar physical properties and transfection efficiency as the PEG7H grafted nanoparticles (Figure S6). SPDP chemistry is useful for ligand conjugation, as sulfhydryl-containing molecules react with high efficiency to the SPDP groups.[59,60] Furthermore, ligand conjugation can be performed following nanoparticle formation, increasing the likelihood that the ligand is effectively presented on the nanoparticle surface as opposed to being embedded in the corona or core of the nanoparticles.

As a proof-of-principle, we conjugated a laminin-derived peptide, RYVVLPR (full sequence Ac-CCRRYVVLPRWLC) to the SPDP terminal groups following nanoparticle formation at a 1:1 molar ratio of thiol in the peptide to SPDP on the nanoparticle surface. This peptide has been previously used to promote neural stem cell adhesion through surface conjugation on various substrates.[61] While it has not previously been used to promote nanoparticle delivery, certain cancer cells, including metastatic prostate cancer cells, up-regulate expression of integrins that bind to laminin.[62−64] Therefore, RYVVLPR peptides may be a unique ligand to enhance lPEI-*g*-PEG/DNA nanoparticle binding to these cancer cells.

Following transfection of PC3-ML cells in vitro, PEG5H-grafted nanoparticles conjugated with RYVVLPR peptides mediated significantly higher transfection efficiency than those without ligands (Figure 4A). Larger increases were observed for 1% and 2.3% PEG grafting degrees, which correlates to nanoparticles with elongated rodlike and wormlike shapes. These results are consistent with reports in the literature showing the importance of elongated shapes for cellular binding when conjugated with specific antibodies targeting breast cancer cells in vitro and lung and tumor tissue in vivo.[65,66] In contrast, when RYVVLPR peptide was conjugated to PEG2K-grafted nanoparticles, no improvement in transfection efficiency was observed for all PEG grafting degrees tested (Figure 4B). All tested conditions displayed near-background levels of transfection efficiency in PC3-ML cells. Although the effect of PEG chain length on cellular uptake differences following ligand conjugation has not been systemically studied in polymeric nanoparticles, a recent study using liposomes reported ligand conjugation to short, 350-Da PEG linkers led to the greatest increase in cell uptake efficiency,[67] corroborating well with our observed results.

DOI: 10.1021/acsbiomaterials.5b00551
ACS Biomater. Sci. Eng. 2016, 2, 567−578

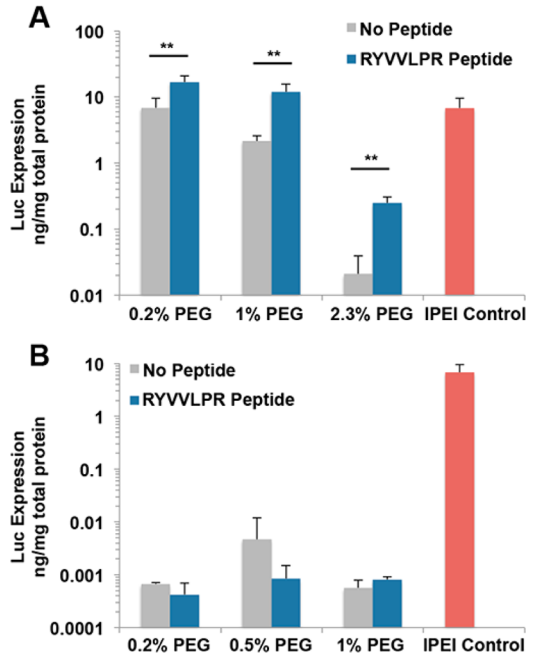

Figure 4. In vitro transfection efficiency following ligand conjugation depends on PEG graft length. Transfection efficiency in PC3 cells mediated by (A) lPEI-*g*-PEG5H/DNA and (B) lPEI-*g*-PEG2K/DNA nanoparticles with and without surface-conjugated cell binding peptide RYVVLPR. Each bar represents mean ± standard deviation (n = 3). ** $p < 0.01$.

To confirm that this result was not specific to this particular ligand or cell type, we conjugated cyclic RGD-thiol peptide (cRGD) to the SPDP terminals and evaluated the transfection efficiency in MDA-MB-231 cells overexpressing integrin $\alpha_v\beta_3$, the specific receptor associated with RGD binding.[68] Results from this study, shown in Figure S7, confirmed the observations in PC3 cells. Ligand-dependent increases in transfection efficiency were only observed when cRGD was conjugated to PEG5H grafts, particularly at 2.3% grafting degree. No significant transgene expression was observed when cRGD peptide was conjugated to nanoparticles with PEG2K grafts.

Importantly, PEG graft length also drastically influenced transfection efficiency following peptide conjugation in vivo. Using Balb/c mice, lPEI-*g*-PEG/DNA nanoparticles conjugated with RYVVLPR peptide were administered via tail vein injection, and the transfection efficiency was analyzed using a luciferase reporter gene. Ligand conjugation did not lead to any increase in gene expression mediated by DNA nanoparticles prepared from lPEI-*g*-PEG with PEG2K grafts, which did not show detectable gene expression. In contrast, nanoparticles with short 1% PEG5H grafts demonstrated significant increase in luciferase expression following conjugation of RYVVLPR peptide (Figure 5). At lower grafting degree (0.2%) for PEG5H grafts, both nanoparticles with or without peptide conjugation showed high levels of transgene expression.

Ligand-Conjugated Nanoparticles with Short PEG Grafts Display Enhanced Transfection Efficiency in Metastatic Prostate Cancer Model. To fully demonstrate the utility of RYVVLPR-conjugated nanoparticles for potential therapeutic applications, we administered lPEI-*g*-PEG/DNA nanoparticles via tail vein injection into PC3-ML tumor-bearing mice, a metastatic prostate cancer model previously used in our lab.[54] For this experiment, the nanoparticles were used to deliver a plasmid DNA encoding firefly luciferase capable of tumor-specific imaging under transcriptional control of the progression-elevated gene-3 promoter (*peg*-Prom).[69,70] The

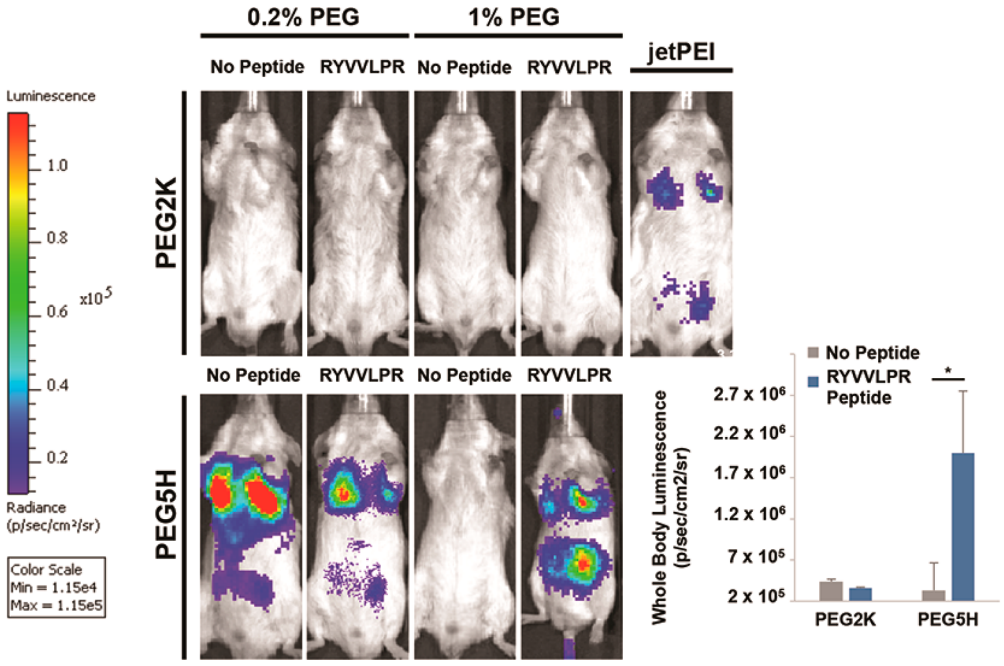

Figure 5. In vivo transfection efficiency following ligand conjugation depends on PEG graft length. In vivo bioluminescence imaging of Balb/c mice 48 h following systemic injection of lPEI-*g*-PEG2K/DNA nanoparticles and lPEI-*g*-PEG5H/DNA nanoparticles prepared without or with RYVVLPR cell adhesion peptide. In vivo jetPEI/DNA nanoparticles were included as control. Plasmid DNA encoding for CMV-driven firefly luciferase was used for all mice. Inset graph depicts quantitative whole-body luciferase expression comparing PEG2K and PEG5H grafted nanoparticles at 1% PEG grafting density. Each bar represents mean ± standard deviation (n = 4). * $p < 0.05$.

DOI: 10.1021/acsbiomaterials.5b00551
ACS Biomater. Sci. Eng. 2016, 2, 567−578

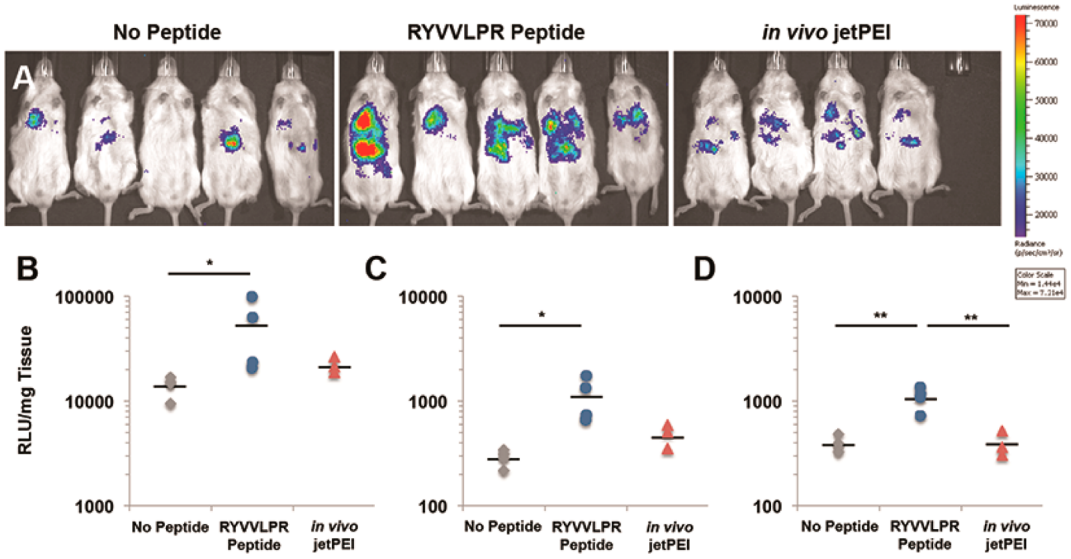

Figure 6. Ligand-conjugated DNA nanoparticles with short PEG5H grafts effectively detect metastatic prostate cancer lesions in vivo. (A) In vivo bioluminescence imaging of PC3-ML tumor-bearing mice at 48 h following systemic injection of lPEI-*g*-PEG/DNA nanoparticles with or without RYVVLPR ligands compared to the positive control, in vivo jetPEI/DNA nanoparticles (n = 4−5 per group). All bioluminescence images were adjusted to the same scale for comparison. (B−D) Comparison of luciferase expression in the (B) lung, (C) liver, and (D) kidney tissue homogenate of the same PC3-ML tumor-bearing mice at 48 h following systemic injection of nanoparticle formulations (n = 3−4 per group). Horizontal bar denotes the mean level of transgene exoression. Plasmid DNA encoding firefly luciferase driven by the tumor-specific *peg*-promoter was used for all experiments. * $p < 0.05$, ** $p < 0.01$.

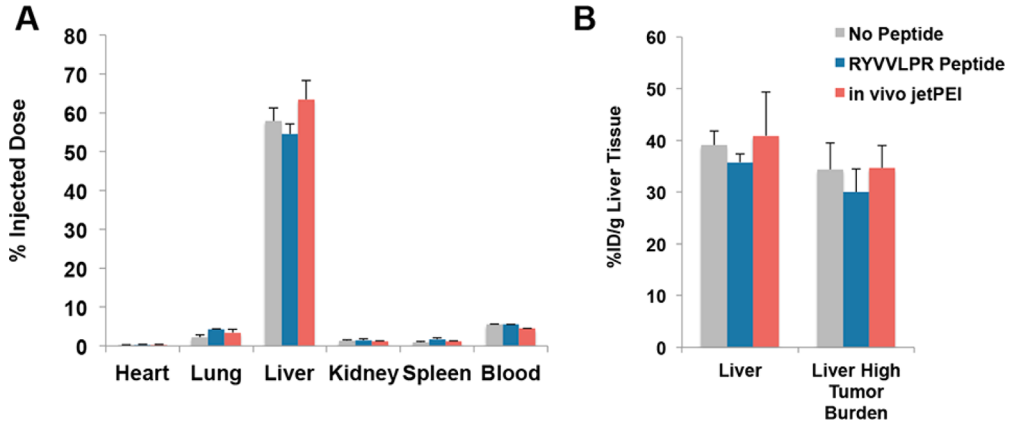

Figure 7. Ligand conjugation does not alter nanoparticle biodistribution in prostate cancer bearing mice. (A) Biodistribution of RYVVLPR-conjugated and unconjugated lPEI-*g*-PEG/DNA nanoparticles and jetPEI control nanoparticles in PC3-ML tumor-bearing mice at 2 h after systemic injection of nanoparticle formulations. (B) Comparison of nanoparticle biodistribution in liver regions with high tumor burden to the general liver as a whole, normalized per gram of liver tissue. Each bar represents mean ± standard deviation (n = 3−4 per group).

peg-Prom constructs have demonstrated tumor-specific gene expression in several experimental cancer models, including breast cancer, melanoma, glioma, and prostate cancer.[54,55,71] The *peg*-Prom-driven transgene expression was only detected in these tumor cells, but not in nontumor tissues, highlighting this approach as a potential for cancer diagnostics. Development of therapeutic or molecular imaging tools for prostate cancer is particularly important, because there are few reliable imaging agents available for clinical applications.

In this model, RYVVLPR-conjugated lPEI-*g*-PEG5H/DNA nanoparticles at 0.2% grafting degree displayed the highest levels of gene expression in organs with high tumor burden: liver, kidney, and lung, in comparison with lPEI-*g*-PEG5H/DNA and in vivo jetPEI control (Figure 6). To quantify the level of gene expression, major organs were collected and homogenized, and firefly luciferase activity was quantified using a luciferase assay. Compared to nanoparticles without ligands, RYVVLPR-conjugation improved gene expression levels by 3.7-fold, 3.9-fold, and 2.8-fold in the lung, liver, and kidney, respectively (Figure 6B−D). Additionally, compared to in vivo jetPEI control nanoparticles, RYVVLPR-conjugated nanoparticles increased expression levels by 2.3-fold, 2.3-fold, and 2.7-fold in the lung, liver, and kidney, respectively. It is important to note that due to the presence of the tumor-specific promoter driving the expression of luciferase marker gene, all detected gene expressions are localized to the PC3-ML psrostate cancer cells. H&E stained tissue sections also confirmed the presence of metastatic lesions in these organs for all treatment groups (Figure S8).

To gain insight into the observed differences in transfection efficiency, we studied the biodistribution of these same set of nanoparticles in PC3-ML tumor bearing mice using tritium-

DOI: 10.1021/acsbiomaterials.5b00551
ACS Biomater. Sci. Eng. 2016, 2, 567−578

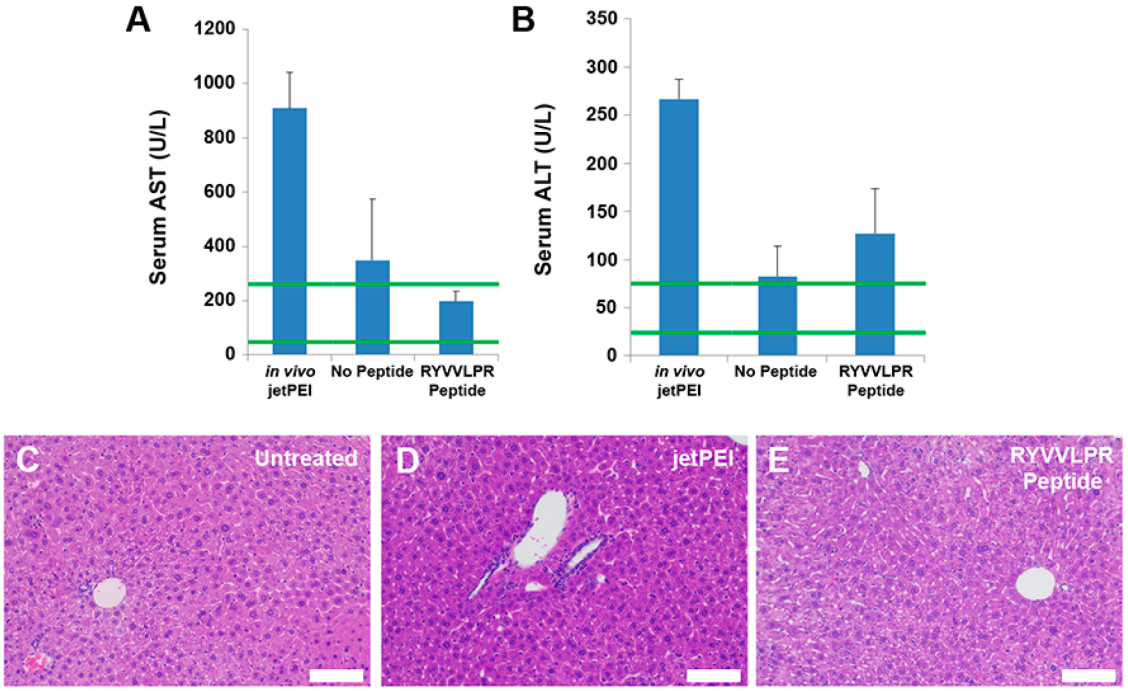

Figure 8. lPEI-*g*-PEG/DNA nanoparticles with short PEG5H grafts show reduced toxicity in vivo. (A, B) Liver enzyme activities analyzed by measuring serum AST (A) and ALT (B) levels in Balb/c mice at 48 h after systemic injection of lPEI-*g*-PEG5H/DNA nanoparticles prepared with or without RYVVLPR cell adhesion peptide and in vivo jetPEI/DNA nanoparticles. Green lines show the normal ranges of AST and ALT enzymes in rats. Each bar represents mean ± standard deviation (n = 4 per group). (C–E) H&E staining of liver tissue comparing untreated controls to those treated with jetPEI/DNA control nanoparticles and RYVVLPR-conjugated lPEI-*g*-PEG5H/DNA nanoparticles. Scale bar represents 100 μm.

labeled DNA. As before, mice were injected intravenously with the nanoparticle formulation; and at 2 h after administration, mice were sacrificed and major organs were harvested. No significant differences in biodistribution were observed between RYVVLPR-conjugated, unconjugated, and in vivo jetPEI control nanoparticles (Figure 7A). In all groups, greater than 50% of the total injected DNA dose accumulated in the liver. Accumulation in the lung was secondary, with 4.2% ± 0.2%, 2.3% ± 0.6%, and 3.4% ± 0.9% of the total injected dose present for RYVVLPR-conjugated, unconjugated, and in vivo jetPEI nanoparticles, respectively. Accumulation in the heart, kidney, and spleen was below 2% for all treatments. Additionally, it is important to note that after 2 h, the majority of the nanoparticles had distributed into the various organs, as less than 5% of the total injected dose remained in the blood. We further analyzed liver biodistribution to determine if nanoparticles showed any preferential accumulation in regions with high tumor burden; however, no significant difference was observed between liver with high tumor burden compared to the whole liver normalized per gram of tissue (Figure 7B). Because of the small size of the lesions in the lung and kidney, similar analysis of tumor and nontumor bearing regions was not possible in these organs. From the results observed in the liver, however, the differences in transfection efficiency among the groups do not appear to be primarily due to differences in biodistribution. Therefore, it is likely that the improvements in transfection efficiency arise from the improved cell binding and uptake mediated by peptide conjugation to the nanoparticle surface.

lPEI-*g*-PEG/DNA Nanoparticles Exhibit Reduced Toxicity in Vivo. In addition to the transfection efficiency improvements, RYVVLPR-conjugated nanoparticles also reduce the toxicity response to nanoparticle treatment in Balb/c mice. We first measured serum levels of aspartate aminotransferase (AST) and alanine aminotransferase (ALT), two common markers of liver function, because a majority of the nanoparticle dose accumulates in the liver. Two days after nanoparticle injection, AST and ALT levels, 900 and 260 U/mL, were significantly higher than the normal range when treated with jetPEI/DNA nanoparticles. RYVVLPR-conjugated nanoparticles, on the other hand, averaged 200 and 120 U/mL for AST and ALT, respectively (Figure 8A, B). We also evaluated tissue morphological changes by H&E staining. In the liver, a mild degree of monocyte accumulation was observed near portal and central veins in mice received in vivo jetPEI/DNA nanoparticles, which correlated well with the elevated ALT and AST levels. Monocyte accumulation was not observed in either lPEI-*g*-PEG/DNA nanoparticle-treated mice or untreated control (Figure 8C).

CONCLUSIONS

In this study, we have demonstrated the importance of short PEG grafts (MW < 1 kDa) for achieving balanced colloidal stability, shape control, and gene transfection efficiency when engineering DNA compacting micellar nanoparticles for systemic delivery. The PEG grafts with MW as low as 500–700 Da (equivalent to an average degree of polymerization of 11.4–16) was effective in conferring shape control ability by varying PEG grafting degree and increasing nanoparticle stability in salt and serum-containing media, displaying reduced surface charges and significantly reduced aggregation, compared to lPEI/DNA control particles. Importantly, short PEG grafts yielded high transfection efficiency for these lPEI-*g*-PEG/DNA micellar nanoparticles with lower in vivo toxicity. Finally, the short PEG grafts were also crucial to realizing the ligand-enhanced transfection activity for these micellar nanoparticles.

DOI: 10.1021/acsbiomaterials.5b00551
ACS Biomater. Sci. Eng. 2016, 2, 567–578

Highlighting the utility and potential therapeutic application of this system, ligand conjugation significantly enhanced lPEI-*g*-PEG/DNA nanoparticle efficiency in a metastatic prostate cancer model only when the short PEG grafts were used as a spacer for ligand conjugation. Taken together, we have identified optimal PEG graft length and terminal groups for lPEI-*g*-PEG/DNA micellar nanoparticles to achieve shape control, high colloidal stability, and high transfection efficiency for in vivo gene delivery applications.

■ ASSOCIATED CONTENT

Supporting Information

The Supporting Information is available free of charge on the ACS Publications website at DOI: 10.1021/acsbiomaterials.5b00551.

^{1}H NMR spectra of lPEI-*g*-PEG copolymer, optimization of N/P ratio, quantification of nanoparticle sizes from TEM images, in vitro transfection in HeLa and MDA-MB-231 cells, DNA release from lPEI-*g*-PEG/DNA nanoparticles, comparison of lPEI-*g*-PEG7H/DNA and lPEI-*g*-PEG5H/DNA nanoparticles, in vitro transfection efficiency following cRGD peptide conjugation, and H&E staining of tumor tissue (PDF)

■ AUTHOR INFORMATION

Corresponding Author

*E-mail: hmao@jhu.edu. Tel: 410-516-8792. Fax: 410-516-5293.

Author Contributions

†J.-M.W. and M.M.A. contributed equally to this work. The manuscript was written through contributions of all authors. All authors have given approval to the final version of the manuscript.

Notes

The authors declare the following competing financial interest(s): Portions of peg-luciferase plasmid expression technology have been licensed by CTS, Inc. Dr. Pomper and Dr. Fisher are co-founders of, serve as consultants to, and have ownership interest in CTS, Inc. Dr. Pomper is a member of the board of directors of CTS, Inc. Johns Hopkins University and Virginia Commonwealth University have ownership interest in CTS, Inc.

■ ACKNOWLEDGMENTS

Funding support for this study was provided by NIH grants R01EB018358, R21EB013274, P50CA058236, and U54CA151838; DOD grant PCRP-W81XWH-14-1-0430;and the Prostate Cancer Foundation A. David Mazzone-PCF Challenge Award.

■ REFERENCES

(1) Ginn, S. L.; Alexander, I. E.; Edelstein, M. L.; Abedi, M. R.; Wixon, J. Gene Therapy Clinical Trials Worldwide to 2012 - an Update. *J. Gene Med.* **2013**, *15*, 65−77.

(2) Hashida, M.; Nishikawa, M.; Yamashita, F.; Takakura, Y. Cell-Specific Delivery of Genes with Glycosylated Carriers. *Adv. Drug Delivery Rev.* **2001**, *52*, 187−196.

(3) Pack, D. W.; Hoffman, A. S.; Pun, S.; Stayton, P. S. Design and Development of Polymers for Gene Delivery. *Nat. Rev. Drug Discovery* **2005**, *4*, 581−593.

(4) Peer, D.; Karp, J. M.; Hong, S.; FaroKhzad, O. C.; Margalit, R.; Langer, R. Nanocarriers as an Emerging Platform for Cancer Therapy. *Nat. Nanotechnol.* **2007**, *2*, 751−760.

(5) Yin, H.; Kanasty, R. L.; Eltoukhy, A. A.; Vegas, A. J.; Dorkin, J. R.; Anderson, D. G. Non-Viral Vectors for Gene-Based Therapy. *Nat. Rev. Genet.* **2014**, *15*, 541−555.

(6) Baum, C.; Kustikova, O.; Modlich, U.; Li, Z.; Fehse, B. Mutagenesis and Oncogenesis By Chromosomal Insertion of Gene Transfer Vectors. *Hum. Gene Ther.* **2006**, *17*, 253−263.

(7) Bessis, N.; GarciaCozar, F. J.; Boissier, M. C. Immune Responses to Gene Therapy Vectors: Influence on Vector Function and Effector Mechanisms. *Gene Ther.* **2004**, *11* (Suppl 1), S10−S17.

(8) Bouard, D.; Alazard-Dany, D.; Cosset, F. L. Viral Vectors: From Virology to Transgene Expression. *Br. J. Pharmacol.* **2009**, *157*, 153−165.

(9) Thomas, C. E.; Ehrhardt, A.; Kay, M. A. Progress and Problems with the Use of Viral Vectors for Gene Therapy. *Nat. Rev. Genet.* **2003**, *4*, 346−358.

(10) Bae, Y. H.; Park, K. Targeted Drug Delivery To Tumors: Myths, Reality and Possibility. *J. Controlled Release* **2011**, *153*, 198−205.

(11) Bertrand, N.; Wu, J.; Xu, X.; Kamaly, N.; Farokhzad, O. C. Cancer Nanotechnology: the Impact of Passive and Active Targeting in the Era of Modern Cancer Biology. *Adv. Drug Delivery Rev.* **2014**, *66*, 2−25.

(12) Chauhan, V. P.; Jain, R. K. Strategies for Advancing Cancer Nanomedicine. *Nat. Mater.* **2013**, *12*, 958−962.

(13) Mura, S.; Nicolas, J.; Couvreur, P. Stimuli-Responsive Nanocarriers for Drug Delivery. *Nat. Mater.* **2013**, *12*, 991−1003.

(14) Park, K. Facing the Truth About Nanotechnology in Drug Delivery. *ACS Nano* **2013**, *7*, 7442−7447.

(15) Harada-Shiba, M.; Yamauchi, K.; Harada, A.; Takamisawa, I.; Shimokado, K.; Kataoka, K. Polyion Complex Micelles as Vectors in Gene Therapy–Pharmacokinetics and In Vivo Gene Transfer. *Gene Ther.* **2002**, *9*, 407−414.

(16) Schaffert, D.; Wagner, E. Gene Therapy Progress and Prospects: Synthetic Polymer-Based Systems. *Gene Ther.* **2008**, *15*, 1131−1138.

(17) Thomas, M.; Klibanov, A. M. Non-Viral Gene Therapy: Polycation-Mediated DNA Delivery. *Appl. Microbiol. Biotechnol.* **2003**, *62*, 27−34.

(18) Davis, M. E. Non-Viral Gene Delivery Systems. *Curr. Opin. Biotechnol.* **2002**, *13*, 128−131.

(19) Goula, D.; Benoist, C.; Mantero, S.; Merlo, G.; Levi, G.; Demeneix, B. A. Polyethylenimine-Based Intravenous Delivery of Transgenes to Mouse Lung. *Gene Ther.* **1998**, *5*, 1291−1295.

(20) Hsu, C. Y.; Uludag, H. Nucleic-Acid Based Gene Therapeutics: Delivery Challenges and Modular Design of Nonviral Gene Carriers and Expression Cassettes to Overcome Intracellular Barriers for Sustained Targeted Expression. *J. Drug Target.* **2012**, *20*, 301−328.

(21) Jones, C. H.; Chen, C. K.; Ravikrishnan, A.; Rane, S.; Pfeifer, B. A. Overcoming Nonviral Gene Delivery Barriers: Perspective and Future. *Mol. Pharmaceutics* **2013**, *10*, 4082−4098.

(22) Morille, M.; Passirani, C.; Vonarbourg, A.; Clavreul, A.; Benoit, J. P. Progress in Developing Cationic Vectors for Non-Viral Systemic Gene Therapy Against Cancer. *Biomaterials* **2008**, *29*, 3477−3496.

(23) Wiethoff, C. M.; Middaugh, C. R. Barriers to Nonviral Gene Delivery. *J. Pharm. Sci.* **2003**, *92*, 203−217.

(24) Bonnet, M.-E.; Erbacher, P.; Bolcato-Bellemin, A.-L. Systemic Delivery of DNA or siRNA Dediated by Linear Polyethylenimine (L-PEI) Does Not Induce an Inflammatory Response. *Pharm. Res.* **2008**, *25*, 2972−2982.

(25) Brissault, B.; Leborgne, C.; Guis, C.; Danos, O.; Cheradame, H.; Kichler, A. Linear Topology Confers In Vivo Gene Transfer Activity to Polyethylenimines. *Bioconjugate Chem.* **2006**, *17*, 759−765.

(26) Kang, Y.; Zhang, X.; Jiang, W.; Wu, C.; Chen, C.; Zheng, Y.; Gu, J.; Xu, C. Tumor-Directed Gene Therapy in Mice Using a Composite Nonviral Gene Delivery System Consisting of the PiggyBac Transposon and Polyethylenimine. *BMC Cancer* **2009**, *9*, 126.

(27) Lavergne, E.; Combadiere, C.; Iga, M.; Boissonnas, A.; Bonduelle, O.; Maho, M.; Debre, P.; Combadiere, B. Intratumoral CC Chemokine Ligand 5 Overexpression Delays Tumor Growth and Increases Tumor Cell Infiltration. *J. Immunol.* **2004**, *173*, 3755−3762.

DOI: 10.1021/acsbiomaterials.5b00551
ACS Biomater. Sci. Eng. 2016, 2, 567−578

(28) Hine, C. M.; Seluanov, A.; Gorbunova, V. Rad51 Promoter-Targeted Gene Therapy is Effective for In Vivo Visualization and Treatment of Cancer. *Mol. Ther.* **2012**, *20*, 347−355.
(29) Jere, D.; Jiang, H. L.; Arote, R.; Kim, Y. K.; Choi, Y. J.; Cho, M. H.; Akaike, T.; Cho, C. S. Degradable Polyethylenimines as DNA and Small Interfering RNA Carriers. *Expert Opin. Drug Delivery* **2009**, *6*, 827−834.
(30) Patnaik, S.; Gupta, K. C. Novel Polyethylenimine-Derived Nanoparticles for In Vivo Gene Delivery. *Expert Opin. Drug Delivery* **2013**, *10*, 215−228.
(31) Itaka, K.; Kataoka, K. Progress and Prospects of Polyplex Nanomicelles for Plasmid DNA Delivery. *Curr. Gene Ther.* **2011**, *11*, 457−465.
(32) Nomoto, T.; Matsumoto, Y.; Miyata, K.; Oba, M.; Fukushima, S.; Nishiyama, N.; Yamasoba, T.; Kataoka, K. In Situ Quantitative Monitoring of Polyplexes and Polyplex Micelles in the Blood Circulation Using Intravital Real-Time Confocal Laser Scanning Microscopy. *J. Controlled Release* **2011**, *151*, 104−109.
(33) Alexis, F.; Pridgen, E.; Molnar, L. K.; Farokhzad, O. C. Factors Affecting the Clearance and Biodistribution of Polymeric Nanoparticles. *Mol. Pharmaceutics* **2008**, *5*, 505−515.
(34) Petersen, H.; Fechner, P. M.; Martin, A. L.; Kunath, K.; Stolnik, S.; Roberts, C. J.; Fischer, D.; Davies, M. C.; Kissel, T. Polyethylenimine-Graft-Poly(ethylene glycol) Copolymers: Influence of Copolymer Block Structure on DNA Complexation and Biological Activities as Gene Delivery System. *Bioconjugate Chem.* **2002**, *13*, 845−854.
(35) Jiang, X.; Qu, W.; Pan, D.; Ren, Y.; Williford, J.-M.; Cui, H.; Luijten, E.; Mao, H.-Q. Plasmid-Templated Shape Control of Condensed DNA−Block Copolymer Nanoparticles. *Adv. Mater.* **2013**, *25*, 227−232.
(36) Williford, J.-M.; Ren, Y.; Huang, K.; Pan, D.; Mao, H.-Q. Shape Transformation Following Reduction-Sensitive PEG Cleavage of Polymer/DNA Nanoparticles. *J. Mater. Chem. B* **2014**, *2*, 8106−8109.
(37) Wei, Z.; Ren, Y.; Williford, J.-M.; Qu, W.; Huang, K.; Ng, S.; Mao, H.-Q.; Luijten, E. Simulation and Experimental Assembly of DNA-Graft Copolymer Micelles with Controlled Morphology. *ACS Biomater. Sci. Eng.* **2015**, *1*, 448−455.
(38) Pozzi, D.; Colapicchioni, V.; Caracciolo, G.; Piovesana, S.; Capriotti, A. L.; Palchetti, S.; De Grossi, S.; Riccioli, A.; Amenitsch, H.; Lagana, A. Effect of Polyethyleneglycol (PEG) Chain Length on the Bio-Nano-Interactions Between PEGylated Lipid Nanoparticles and Biological Fluids: from Nanostructure to Uptake in Cancer Cells. *Nanoscale* **2014**, *6*, 2782−2792.
(39) Hatakeyama, H.; Akita, H.; Harashima, H. A Multifunctional Envelope Type Nano Device (MEND) for Gene Delivery to Tumours Based on the EPR Effect: a Strategy for Overcoming the PEG Dilemma. *Adv. Drug Delivery Rev.* **2011**, *63*, 152−160.
(40) Ge, Z. S.; Chen, Q. X.; Osada, K.; Liu, X. Y.; Tockary, T. A.; Uchida, S.; Dirisala, A.; Ishii, T.; Nomoto, T.; Toh, K.; Matsumoto, Y.; Oba, M.; Kano, M. R.; Itaka, K.; Kataoka, K. Targeted Gene Delivery by Polyplex Micelles with Crowded PEG Palisade and cRGD Moiety for Systemic Treatment of Pancreatic Tumors. *Biomaterials* **2014**, *35*, 3416−3426.
(41) Chauhan, V. P.; Popovic, Z.; Chen, O.; Cui, J.; Fukumura, D.; Bawendi, M. G.; Jain, R. K. Fluorescent Nanorods and Nanospheres for Real-Time In Vivo Probing of Nanoparticle Shape-Dependent Tumor Penetration. *Angew. Chem., Int. Ed.* **2011**, *50*, 11417−11420.
(42) Geng, Y.; Dalhaimer, P.; Cai, S.; Tsai, R.; Tewari, M.; Minko, T.; Discher, D. E. Shape Effects of Filaments Versus Spherical Particles in Flow and Drug Delivery. *Nat. Nanotechnol.* **2007**, *2*, 249−255.
(43) Gratton, S. E. A.; Ropp, P. A.; Pohlhaus, P. D.; Luft, J. C.; Madden, V. J.; Napier, M. E.; DeSimone, J. M. The Effect of Particle Design on Cellular Internalization Pathways. *Proc. Natl. Acad. Sci. U. S. A.* **2008**, *105*, 11613−11618.
(44) Williford, J.-M.; Santos, J. L.; Shyam, R.; Mao, H.-Q. Shape Control in Engineering of Polymeric Nanoparticles for Therapeutic Delivery. *Biomater. Sci.* **2015**, *3*, 894−907.
(45) Klutz, K.; Schaffert, D.; Willhauck, M. J.; Grunwald, G. K.; Haase, R.; Wunderlich, N.; Zach, C.; Gildehaus, F. J.; Senekowitsch-Schmidtke, R.; Goke, B.; Wagner, E.; Ogris, M.; Spitzweg, C. Epidermal Growth Factor Receptor-Targeted (131)I-Therapy of Liver Cancer Following Systemic Delivery of the Sodium Iodide Symporter Gene. *Mol. Ther.* **2011**, *19*, 676−685.
(46) Rodl, W.; Schaffert, D.; Wagner, E.; Ogris, M. Synthesis of Polyethylenimine-Based Nanocarriers for Systemic Tumor Targeting of Nucleic Acids. *Methods Mol. Biol.* **2013**, *948*, 105−120.
(47) Osada, K. Development of Functional Polyplex Micelles for Systemic Gene Therapy. *Polym. J.* **2014**, *46*, 469−475.
(48) Yang, J.; Hendricks, W.; Liu, G. S.; McCaffery, J. M.; Kinzler, K. W.; Huso, D. L.; Vogelstein, B.; Zhou, S. B. A Nanoparticle Formulation that Selectively Transfects Metastatic Tumors in Mice. *Proc. Natl. Acad. Sci. U. S. A.* **2013**, *110*, 14717−14722.
(49) Erbacher, P.; Bettinger, T.; Belguise-Valladier, P.; Zou, S. M.; Coll, J. L.; Behr, J. P.; Remy, J. S. Transfection and Physical Properties of Various Saccharide, Poly(ethylene glycol), and Antibody-Derivatized Polyethylenimines (PEI). *J. Gene Med.* **1999**, *1*, 210−222.
(50) Blessing, T.; Kursa, M.; Holzhauser, R.; Kircheis, R.; Wagner, E. Different Strategies for Formation of Pegylated EGF-Conjugated PEI/DNA Complexes for Targeted Gene Delivery. *Bioconjugate Chem.* **2001**, *12*, 529−537.
(51) Knorr, V.; Allmendinger, L.; Walker, G. F.; Paintner, F. F.; Wagner, E. An Acetal-Based PEGylation Reagent for pH-Sensitive Shielding of DNA Polyplexes. *Bioconjugate Chem.* **2007**, *18*, 1218−1225.
(52) Namgung, R.; Kim, J.; Singha, K.; Kim, C. H.; Kim, W. J. Synergistic Effect of Low Cytotoxic Linear Polyethylenimine and Multiarm Polyethylene Glycol: Study of Physicochemical Properties and In Vitro Gene Transfection. *Mol. Pharmaceutics* **2009**, *6*, 1826−1835.
(53) Ren, Y.; Jiang, X. A.; Pan, D.; Mao, H. Q. Charge Density and Molecular Weight of Polyphosphoramidate Gene Carrier Are Key Parameters Influencing Its DNA Compaction Ability and Transfection Efficiency. *Biomacromolecules* **2010**, *11*, 3432−3439.
(54) Bhatnagar, A.; Wang, Y. C.; Mease, R. C.; Gabrielson, M.; Sysa, P.; Minn, I.; Green, G.; Simmons, B.; Gabrielson, K.; Sarkar, S.; Fisher, P. B.; Pomper, M. G. AEG-1 Promoter-Mediated Imaging of Prostate Cancer. *Cancer Res.* **2014**, *74*, 5772−5781.
(55) Bhang, H. E. C.; Gabrielson, K. L.; Laterra, J.; Fisher, P. B.; Pomper, M. G. Tumor-Specific Imaging Through Progression Elevated Gene-3 Promoter-Driven Gene Expression. *Nat. Med.* **2011**, *17*, 123−129.
(56) Li, Y.; Kroger, M.; Liu, W. K. Endocytosis of PEGylated Nanoparticles Accompanied by Structural and Free Energy Changes of the Grafted Polyethylene Glycol. *Biomaterials* **2014**, *35*, 8467−8478.
(57) Mishra, S.; Webster, P.; Davis, M. E. PEGylation Significantly Affects Cellular Uptake and Intracellular Trafficking of Non-Viral Gene Delivery Particles. *Eur. J. Cell Biol.* **2004**, *83*, 97−111.
(58) Zhong, Y.; Meng, F.; Deng, C.; Zhong, Z. Ligand-Directed Active Tumor-Targeting Polymeric Nanoparticles for Cancer Chemotherapy. *Biomacromolecules* **2014**, *15*, 1955−1969.
(59) Carlsson, J.; Drevin, H.; Axen, R. Protein Thiolation and Reversible Protein-Protein Conjugation. N-Succinimidyl 3-(2-pyridyldithio)propionate, a New Heterobifunctional Reagent. *Biochem. J.* **1978**, *173*, 723−737.
(60) Hermanson, G. T. *Bioconjugate Techniques*, 3rd ed.; Academic: Cambridge, MA, 2013; pp 1−1146.
(61) Li, X.; Liu, X.; Josey, B.; Chou, C. J.; Tan, Y.; Zhang, N.; Wen, X. Short Laminin Peptide for Improved Neural Stem Cell Growth. *Stem Cells Transl. Med.* **2014**, *3*, 662−670.
(62) Dedhar, S.; Saulnier, R.; Nagle, R.; Overall, C. M. Specific Alterations in the Expression of Alpha-3-Beta-1 and Alpha-6-Beta-4 Integrins in Highly Invasive and Metastatic Variants of Human Prostate Carcinoma-Cells Selected by in-Vitro Invasion through Reconstituted Basement-Membrane. *Clin. Exp. Metastasis* **1993**, *11*, 391−400.

DOI: 10.1021/acsbiomaterials.5b00551
ACS Biomater. Sci. Eng. 2016, 2, 567−578

(63) King, T. E.; Pawar, S. C.; Majuta, L.; Sroka, I. C.; Wynn, D.; Demetriou, M. C.; Nagle, R. B.; Porreca, F.; Cress, A. E. The Role of Alpha 6 Integrin in Prostate Cancer Migration and Bone Pain in a Novel Xenograft Model. *PLoS One* **2008**, *3*, e3535.
(64) Nagle, R. B.; Hao, J. S.; Knox, J. D.; Dalkin, B. L.; Clark, V.; Cress, A. E. Expression of Hemidesmosomal and Extracellular-Matrix Proteins by Normal and Malignant Human Prostate Tissue. *Am. J. Pathol.* **1995**, *146*, 1498−1507.
(65) Barua, S.; Yoo, J. W.; Kolhar, P.; Wakankar, A.; Gokarn, Y. R.; Mitragotri, S. Particle Shape Enhances Specificity of Antibody-Displaying Nanoparticles. *Proc. Natl. Acad. Sci. U. S. A.* **2013**, *110*, 3270−3275.
(66) Kolhar, P.; Anselmo, A. C.; Gupta, V.; Pant, K.; Prabhakarpandian, B.; Ruoslahti, E.; Mitragotri, S. Using Shape Effects to Target Antibody-Coated Nanoparticles to Lung and Brain Endothelium. *Proc. Natl. Acad. Sci. U. S. A.* **2013**, *110*, 10753−10758.
(67) Stefanick, J. F.; Ashley, J. D.; Kiziltepe, T.; Bilgicer, B. A Systematic Analysis of Peptide Linker Length and Liposomal Polyethylene Glycol Coating on Cellular Uptake of Peptide-Targeted Liposomes. *ACS Nano* **2013**, *7*, 2935−2947.
(68) Shallal, H. M.; Minn, I.; Banerjee, S. R.; Lisok, A.; Mease, R. C.; Pomper, M. G. Heterobivalent Agents Targeting PSMA and Integrin-alphavbeta3. *Bioconjugate Chem.* **2014**, *25*, 393−405.
(69) Su, Z. Z.; Sarkar, D.; Emdad, L.; Duigou, G. J.; Young, C. S.; Ware, J.; Randolph, A.; Valerie, K.; Fisher, P. B. Targeting gene expression selectively in cancer cells by using the progression-elevated gene-3 promoter. *Proc. Natl. Acad. Sci. U. S. A.* **2005**, *102*, 1059−1064.
(70) Su, Z. Z.; Shi, Y.; Fisher, P. B. Subtraction hybridization identifies a transformation progression-associated gene PEG-3 with sequence homology to a growth arrest and DNA damage-inducible gene. *Proc. Natl. Acad. Sci. U. S. A.* **1997**, *94*, 9125−9130.
(71) Minn, I.; Bar-Shir, A.; Yarlagadda, K.; Bulte, J. W.; Fisher, P. B.; Wang, H.; Gilad, A. A.; Pomper, M. G. Tumor-specific expression and detection of a CEST reporter gene. *Magn. Reson. Med.* **2015**, *74*, 544−549.

DOI: 10.1021/acsbiomaterials.5b00551
ACS Biomater. Sci. Eng. 2016, 2, 567−578